Geochemical Perspectives Letters

Dating recent aqueous activity on Mars

M.M. Tremblay, D.F. Mark, D.N. Barfod, B.E. Cohen, R.B. Ickert, M.R. Lee, T. Tomkinson, and C.L. Smith

Supplementary Information

The Supplementary Information includes:

- Alteration Phases in Lafayette
- Recalculation and Reinterpretation of Rb-Sr Systematics in Martian Meteorites Lafayette and Yamato (Y) 000593
- Micro-encapsulation $^{40}Ar/^{39}Ar$ Methods
- Argon Diffusion Calculations
- Figures S-1 to S-3
- Tables S-1 to S-3
- Supplementary Information References

Alteration Phases in Lafayette

The alteration phases present in Lafayette, which we collectively refer to as "iddingsite," and in the nakhlite meteorites more generally, have been extensively studied and described (*e.g.*, Bridges and Grady, 2000; Bridges *et al.*, 2019; Changela and Bridges, 2010; Gyollai *et al.*, 2023; Hicks *et al.*, 2014; Krämer Ruggiu *et al.*, 2020; Lee *et al.*, 2013, 2015, 2018; Martínez *et al.*, 2023; McCubbin *et al.*, 2009; Piercy *et al.*, 2022; Tomkinson *et al.*, 2013; Treiman, 2005; Treiman *et al.*, 1993). Here, we summarize some of the key mineralogical and textural observations that are of relevance for understanding our $^{40}Ar/^{39}Ar$ dates of the alteration phases in Lafayette.

The abundance, and to a lesser degree the mineralogy, of the alteration phases in Lafayette are documented to be variable across different samples or aliquots of the meteorite (*e.g.*, Piercy *et al.*, 2022). The aliquots of iddingsite that we separated for $^{40}Ar/^{39}Ar$ geochronology were taken from the same material that Tomkinson *et al.* (2013) and Lee *et al.* (2015) studied, so we focus on their characterization here. They documented that both narrow (1-2 μm) and wide (up to 40 μm) olivine-hosted veins contain finely crystallised Fe-Mg silicate identified as saponite (Tomkinson *et al.*, 2013). In the wider veins, the saponite is observed to be mantled by Fe-rich smectite phyllosilicates (*e.g.*, Treiman *et al.*, 1993) or intergrown smectite and serpentine (*e.g.*, Changela and Bridges, 2010), and in some of the widest veins siderite is also observed (*e.g.*, Tomkinson *et al.*, 2013; Lee *et al.*, 2015). Lee *et al.* (2015) interpreted the mineral assemblage in the olivine-hosted veins to reflect a multistage process, with the saponite crystallising and filling in fractures first, followed by the incongruent dissolution of the vein walls and replacement by siderite, which was finally replaced by the smectite or intergrown smectite and serpentine. While we were not able to differentiate between these major alteration phases when we physically separated the vein-filling alteration material from their olivine grain hosts, we anticipate based on mineralogy that the phyllosilicates will dominate the K budget responsible for production of radiogenic ^{40}Ar.

A multi-stage formation history of the iddingsite mineral assemblage in Lafayette (*e.g.*, Lee *et al.*, 2015) is consistent with detailed petrologic studies of the alteration assemblages in other nakhlites (*e.g.*, Changela and Bridges, 2010; Lee *et al.*, 2013; Gyollai *et al.*, 2023; Martínez *et al.*, 2023). Although we report the most precise date for these alteration phases in Lafayette to date, it is worth noting that the age we obtain of 742 Ma still has a nontrivial uncertainty of 15 Ma (2σ). Therefore, a multi-stage formation history of the alteration mineral assemblage is certainly permissible within the age window and could be significantly shorter (*e.g.*, Changela and Bridges, 2010), but this possibility is not currently resolvable *via* radiometric dating alone.

Recalculation and Reinterpretation of Rb-Sr Systematics in Martian Meteorites Lafayette and Yamato (Y) 000593

The most widely cited constraint on the timing of iddingsite formation in the nakhlites derives from the Rb-Sr systematics of acid-leachates from the meteorites Lafayette and Yamato (Y) 000593 (Shih *et al.*, 1998; Misawa *et al.*, 2005). The Rb-Sr data from Lafayette were only presented in a small figure in an abstract (Shih *et al.*, 1998). To reevaluate these data, we digitized the Rb-Sr data, as well as the Sm-Nd data, from the figures in Shih *et al.* (1998), including the uncertainties. Because the Rb-Sr data for Lafayette and Y000593 were combined by Borg and Drake (2005) to infer an age for iddingsite in the nakhlites, we also re-reduced the radioisotopic data (Rb-Sr and Sm-Nd) from both Lafayette (Shih *et al.*, 1998) and Y000593 (Misawa *et al.*, 2005) using a consistent calculation approach.

The radioisotopic data from Shih *et al.* (1998) were derived from a crushed, 0.5 g sample of Lafayette. We briefly summarize their methods here. Before separation, three whole rock aliquots (WR, WR1, WR2) were separated from the crushed sample. After WR separation, a pyroxene (Px) and an olivine (Ol) separate were picked by hand, as were two different "iddingsite" fragments (Id1 and Id2; described as a composite mixture of alteration materials, olivine and pyroxene). All aliquots except WR1 and WR2 were leached in 1 mol/L HCl. All leachates and residues, and the two unleached WR aliquots, were measured for their Rb, Sr, and Sr isotopic compositions. The methods used by Misawa *et al.* (2005) are very similar, with the exception that they used 2 mol/L HCl.

Digitization and new calculations of Rb-Sr and Sm-Nd systematics

There are line elements behind the data points in the vector figure of Shih *et al.* (1998) that we interpret as uncertainty bars. We interpret the uncertainties to be plotted at the 2σ level, because they are similar in magnitude to the reported 2σ uncertainties in Shih *et al.* (1999) on the nakhlite Governador Valadares, which were made using the same analytical methods in the same lab at around the same time. These values are reported in Table S-1. The original isochron-style regressions used what are now outdated implementations of line-fitting algorithms that are difficult or impossible to reproduce, and which may have been adjusted in ways that are not well documented (*cf.* discussion in Nyquist *et al.*, 1986). As a result, we have recalculated linear fits using a widely used and reproducible algorithm from York *et al.*, (2004). This algorithm underpins the default line-fitting method in Isoplot (Ludwig, 2008) and IsoplotR (Vermeesch, 2018). The uncertainties we report are based on propagating the *a priori* analytical uncertainties only, and no adjustment has been made to account for overdispersion. To compare our calculations to the originally reported values, we use the decay constants from the original publications ($\lambda_{87Rb} = 1.390 \cdot 10^{-11}$ a^{-1} for Shih *et al.* (1998) and $1.402 \cdot 10^{-11}$ a^{-1} for Misawa *et al.* (2005); and $\lambda_{147Sm} = 6.540 \cdot 10^{-12}$ a^{-1} for both). The difference between ages calculated with the two ^{87}Rb decay constants is ~11 Myr.

Using the digitized data for Lafayette and excluding the leachates from Id1 and Id2, as was done by Shih *et al.* (1998), the Rb-Sr data yield a line with a slope corresponding to a date of 1.281 ± 0.021 Ga and an intercept of 0.70259 ± 0.00004 (2σ; n = 10; MSWD = 23.4; Fig. S-1), compared to the published values of 1.26 ± 0.07 Ga and 0.70260 ± 0.00014 (no sigma level or MSWD were originally reported). To confirm the accuracy of our digitization, we also calculate an Sm-Nd age and intercept from the digitized data of 1.317 ± 0.033 Ga (2σ; n = 11; MSWD = 2.3) and initial

εNd of 16.3 ± 0.6, compared to the published values of 1.32 ± 0.05 Ga and initial εNd of 16.3 ± 0.4 (Shih *et al.*, 1998). These new values are summarized in Table S-1.

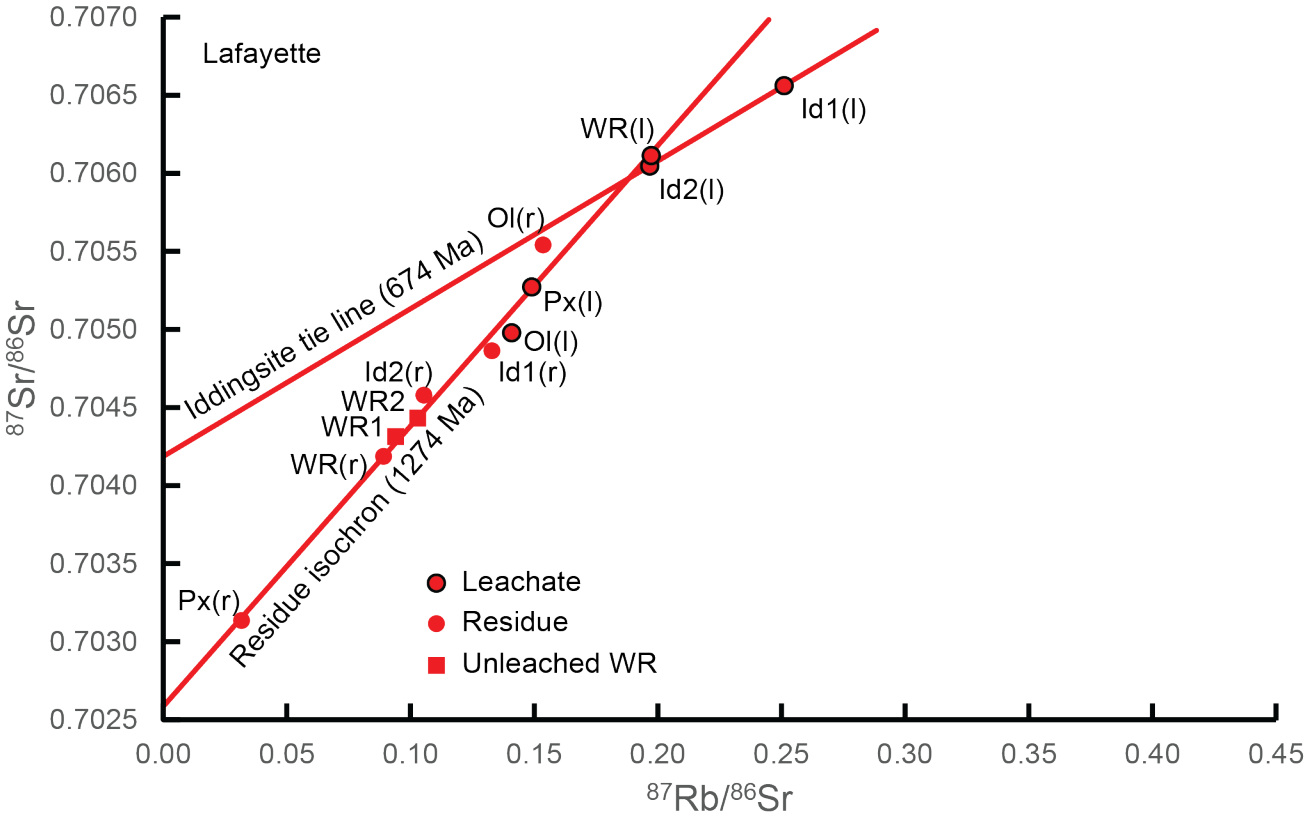

Figure S-1 Isochron style plot of Rb-Sr data from the meteorite Lafayette. Data has been digitized from the original figure of Shih *et al.* (1998). Uncertainties are smaller than the symbols plotted.

For consistency, we also re-reduced the data from Misawa *et al.* (2005) on Y000593. Using the same 5 aliquots for Rb-Sr as the authors (WR1, WR(r), Cpx(r), Cpx2(r), and NMag(r)), we calculate a line with a slope corresponding to a date of 1.302 ± 0.024 Ga and an intercept of 0.702524 ± 0.000027 (2σ; n = 5; MSWD = 3.1; Fig. S-1) compared with the published values of 1.30 ± 0.02 Ga and 0.702525 ± 0.000027 (no sigma level). For Sm-Nd, we use the same 6 samples as the authors (WR1, WR(r), WR(l), Cpx(r), Cpx(l), and Cpx2(r)) and recover a line with a slope corresponding to a date of 1.314 ± 0.018 Ga and initial εNd of 15.8 ± 0.4 (2σ; n = 6; MSWD = 4.8), compared to the published values of 13.1 ± 0.03 Ga and 16.0 ± 0.2 (no sigma level reported). These new values are summarized in Table S-1.

The results from the digitized data agree with the results presented by Shih *et al.* (1998) for Lafayette and for Y000593 presented by Misawa *et al.* (2005), which suggests that the digitization is broadly accurate. The larger uncertainties for some aliquots in the original publications appear to scale with the degree of overdispersion, and most likely are derived from an undescribed effort to account for non-analytical scatter (*cf.* Nyquist *et al.*, 1986). Calculating an MSWD makes clear that the Rb-Sr data of Lafayette are significantly overdispersed, implying a disturbance in the Rb-Sr systematics.

Reinterpretation of the Rb-Sr Systematics

The chronological information on timing of alteration of the nakhlites has previously been derived from four analyses, two each from Lafayette and Y000593 (Borg and Drake, 2005). From Lafayette, the two leachates were from separates

Id1 and Id2, the composite mixtures of primary igneous minerals and alteration material. From Y000593, the leachates are from two olivine separates, one from the 3.6-3.95 g/cm^3 fraction (Ol(l)), and one from the fraction denser than 3.95 g/cm^3, called ρ > 3.95. Each pair was regressed as a two-point model isochron. Recalculating a slope and intercept from each data pair yields apparent dates and initial Sr isotope compositions, at 2σ, of 677 ± 68 Ma and 0.7042 ± 0.0002 for Lafayette, and 650 ± 80 Ma and 0.7046 ± 0.0001 for Y000593. These recalculated values agree well with the original published values of 679 ± 66 Ma and 650 ± 80 Ma, respectively. Calculating the ages relative to a common decay constant (Rotenberg *et al.*, 2012) yields 674 ± 68 Ma for Lafayette and 653 ± 80 Ma for Y000593 (Figs. S-1 and S-2). Note that the Borg and Drake (2005) compilation also includes an additional date from Y000593 of 614 ± 29 Ma from the olivine residues based on a preliminary presentation of the data in an abstract (Shih *et al.*, 2002). However, the residual data later updated in Misawa *et al.* (2005) cannot be interpreted that way: the two olivine residue pairs have a negative slope on an isochron-style plot. Unfortunately, the uncorrected data from the residues reported originally (Shih *et al.*, 2002) were included as the most precise value in the weighted mean age for alteration in the nakhlites reported by Borg and Drake (2005), and therefore dominates their value.

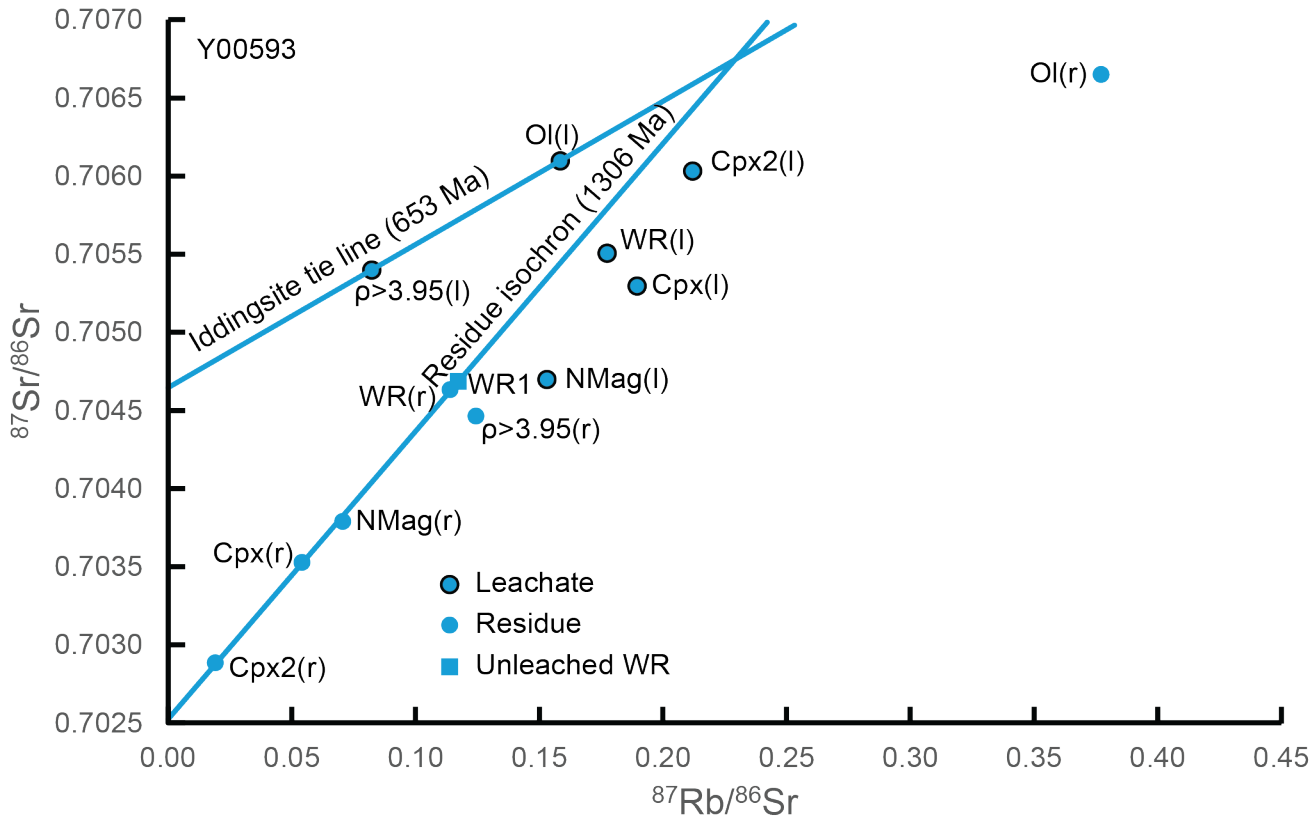

Figure S-2 Isochron style plot of Rb-Sr data from the meteorite Y000593. Data are from Misawa *et al.* (2005). Uncertainties are smaller than the symbols plotted.

There is no discussion of the chronological significance of the Lafayette two-point tie line apparent date in Shih *et al.* (1998). It is notable that the leached olivine separate from Lafayette, Ol(l), which presumably also contains iddingsite, does not plot near the slope of the Id1(l)-Id2(l) tie line (Fig. S-1). In Misawa *et al.* (2005), the discussion of Y000593 is framed speculatively, putting the word age, when associated with this two-point isochron, in quotation marks.

A two point model isochron provides no indication as to whether the Rb-Sr system has been disturbed. The only firm constraints provided by such a model are whether the data are non-physical, such if the linear fit had a negative

slope, or unlikely, such as if the linear fit had a slope in excess of 0.066, which would indicate a presolar date, or correspond to an impossible or unlikely intercept (*e.g.*, $^{87}Sr/^{86}Sr < 0.698$). Beyond these constraints, two-point linear fits allow for a wide range of possible Rb-Sr systematics, and do not preclude the possibility of minor disturbances that result in a small but significant change in the slope and therefore apparent date. This is why having many points with a large range in parent/daughter is widely considered necessary for a robust isochron.

One process that could have disturbed the measured ratio of Rb to Sr (and therefore moved the aliquots along the x-axis of the isochron-style diagram) is the analytical approach itself. The leaching experiments done by Shih *et al.* (1998) and Misawa *et al.* (2005) consist of a light agitation in a weak HCl solution. Fractionation of chemical compositions is common during geo- or cosmo-chemical leaching procedures if the entire sample is not digested, particularly when the elements have different chemical behaviour or one is a radiogenic daughter product incompatible in the host (*e.g.*, Mattinson, 1994). This was documented in the experiments by Clauer *et al.* (1993) who leached *ca.* 500 Ma clay minerals in a variety of reagents and measured the Rb-Sr systematics. They demonstrated that 1 mol/L HCl could produce leachates that fractionated Rb and Sr and led to the leachate Rb-Sr and $^{87}Sr/^{86}Sr$ systematics that plotted on linear arrays that did not correspond to accurate ages.

At present, the two tie line slopes from Lafayette and Y000593 are indistinguishable at a ~10 % precision. Whether or not this is a coincidence remains to be seen, and the data indicate that investigating the Rb-Sr systematics of the alteration minerals in the nakhlites might be a fruitful avenue for future work to determine their chronological significance.

Micro-encapsulation $^{40}Ar/^{39}Ar$ Methods

The 0.216 g sample of Lafayette we obtained from the Smithsonian Museum was crushed to 63-125 µm, split into 12 different ~50 mg aliquots, and disaggregated in an ultrasonic bath for 30 minutes, breaking apart grains and separating the iddingsite from their host olivine and pyroxene grains. These grains were examined using a binocular microscope, and any iddingsite adhering to mineral surfaces was scraped off using a fine stainless-steel needle, then manually picked. Aliquots of iddingsite, each weighing *ca.* 1 µg, were prepared for neutron irradiation.

To micro-encapsulate these 12 iddingsite aliquots, we wrapped each aliquot in Cu foil packets positioned within 2 cm-diameter quartz glass tubes, connected to a glass tree on a vacuum line fitted with a glass cold finger. The cold finger was cooled by liquid nitrogen to –196 °C and the glass tube was evacuated. The glass tube was evacuated by a Pfeiffer diaphragm-backed turbomolecular pumping-station and an ion pump (the latter switched on once the system had achieved 10^{-7} mbar). Once a pressure gauge indicated a base pressure better than 2×10^{-9} mbar, the glass tube was flame heated and the sample sealed within the glass capsule. The 12 glass capsules were positioned within a large glass vial along with neutron-fluence monitor Hb3gr (1081.0 ± 1.2 Ma, 1σ; Renne *et al.*, 2011), and secondary standard GA1550 (99.738 ± 0.104 Ma, 1σ; Renne *et al.*, 2011). Samples were then irradiated for 80 hours in the Cd-lined TRIGA facility, Oregon State University, USA.

After a decay period of 4 to 5 months following neutron irradiation, analyses of neutron flux monitors and Lafayette iddingsite aliquots were made in the NERC Argon Isotope Facility, Scottish Universities Environmental Research Centre (SUERC), with a Thermo Scientific HELIX-SFT spectrometer fitted with an ion counting Balzers SEV-217 electron multiplier (measurement of ^{39}Ar-^{36}Ar) and a 10^{12} Ohm resistor Faraday (measurement of ^{40}Ar). Owing to the potential temperature sensitivity of the iddingsite, the material was only baked at 40 °C for 96 hours in an ultra-high vacuum laser cell. Isotope measurements were performed in peak-hopping mode, with a measured sensitivity of 1.13×10^{-13} moles per Volt. Hb3gr crystals were analysed *via* total-fusion and GA1550 crystals were step-heated. All data are reported relative to the J-parameter calculated from measurements of GA1550.

The glass capsules were cracked sequentially in vacuum with a custom-built tube cracker that involves dropping a magnetic ball bearing onto the swan necks of the glass tubes, and the ^{37}Ar and ^{39}Ar was measured. The ^{40}Ar, ^{38}Ar and ^{36}Ar were also measured as a check that neither the bakeout procedure nor the irradiation liberated radiogenic ^{40}Ar from the iddingsite. Beyond small components of terrestrial atmospheric Ar, which is readily detected by its $^{40}Ar/^{36}Ar$ ratio

(Table S-2), there was no evidence of degassing of radiogenic ^{40}Ar. The small copper packets were subsequently extracted from the broken capsules and the samples were fused using a Teledyne 75 W diode laser defocused over the sample using a 2.5 mm spot size and between 30 and 50 % laser power. All released gases were purified using two SAES GP50 getters with ST101 Zr-Al cartridges, one at room temperature and the other at 450 °C. Isotope extraction, purification, extraction line operation and mass spectrometry were fully automated using *MassSpec* software version 8.131.

The ^{37}Ar and ^{39}Ar measurements from the cracked vials were added to the bulk isotope measurements (^{36}Ar-^{40}Ar) and data were corrected for background measurements, mass discrimination, and radioactive decay since irradiation the using *MassSpec* software. The data were also corrected for cosmogenic argon using a combination of the meteorite's cosmogenic exposure age (10.7 ± 0.4 Ma; Cohen *et al.*, 2017), assuming no pre-ejection exposure, and the ^{38}Ar and ^{36}Ar cosmogenic production rates calculated from the Ca/K values measured on each ^{40}Ar/^{39}Ar measurement using the approach of Cassata and Borg (2016), as well as for Martian atmosphere using the trapped ^{40}Ar/^{36}Ar component of 1520 ± 200 (1σ) previously determined by Cohen *et al.* (2017). This measurement was used to correct for Martian atmospheric contribution. The data exhibit a tight clustering on an isotope correlation plot, prohibiting the use of an isochron approach to determine an initial ^{40}Ar/^{36}Ar trapped component composition directly from the iddingsite. We report ages with both analytical precision followed by full external precision, with the latter including uncertainties from the decay constant, at 2-sigma confidence. Ages were calculated using the optimization model of Renne *et al.* (2010) and the parameters of Renne *et al.* (2011). Values used in the ^{40}Ar/^{39}Ar data reduction are listed in Table S-2, and measured argon isotopic data are reported in Table S-3.

The ^{40}Ar/^{39}Ar age we obtain for iddingsite in Lafayette is coincident with most of the initial, low temperature heating steps for the different nakhlites reported by Cohen *et al.* (2017), as is the $^{38}Ar_{Cl}$ enrichment. This observation supports the interpretation that the low temperature extraction steps in most of the bulk rock nakhlite ^{40}Ar/^{39}Ar age spectra define a mixing relationship between a young K-bearing iddingsite and the older magmatic constituents (Fig. S-3). The increasing age with increasing cumulative $^{39}Ar_K$ release is independent of irradiation duration and is correlated with $^{38}Ar_{Cl}$. We know from neutron irradiation of the iddingsite that these samples are susceptible to ^{37}Ar and ^{39}Ar recoil and the significantly younger age steps likely reflect recoil, as previously suggested (Burgess *et al.*, 2000). The observation of young initial age spectra steps associated with alteration of an older igneous rock is also supported by similar distributions in the age spectra of altered terrestrial samples (*e.g.*, Mark *et al.*, 2011). The low temperature diffusive profiles detailed by Cassata *et al.* (2010) for Nakhla are likely masked by the data of Cohen *et al.* (2017) as they did not date pyroxene and plagioclase separates, and instead dated whole rock material, which included a younger iddingsite age component. Moreover, the observation that ^{40}Ar/^{39}Ar ages decrease with increasing $^{38}Ar_{Cl}$ (Fig. S-3), alongside with the good agreement between the ^{40}Ar/^{39}Ar ages of the 12 iddingsite aliquots we measured, argues against the presence of any excess argon in fluid inclusions within the iddingsite (*e.g.*, Harrison *et al.*, 1994; Kelley, 2002).

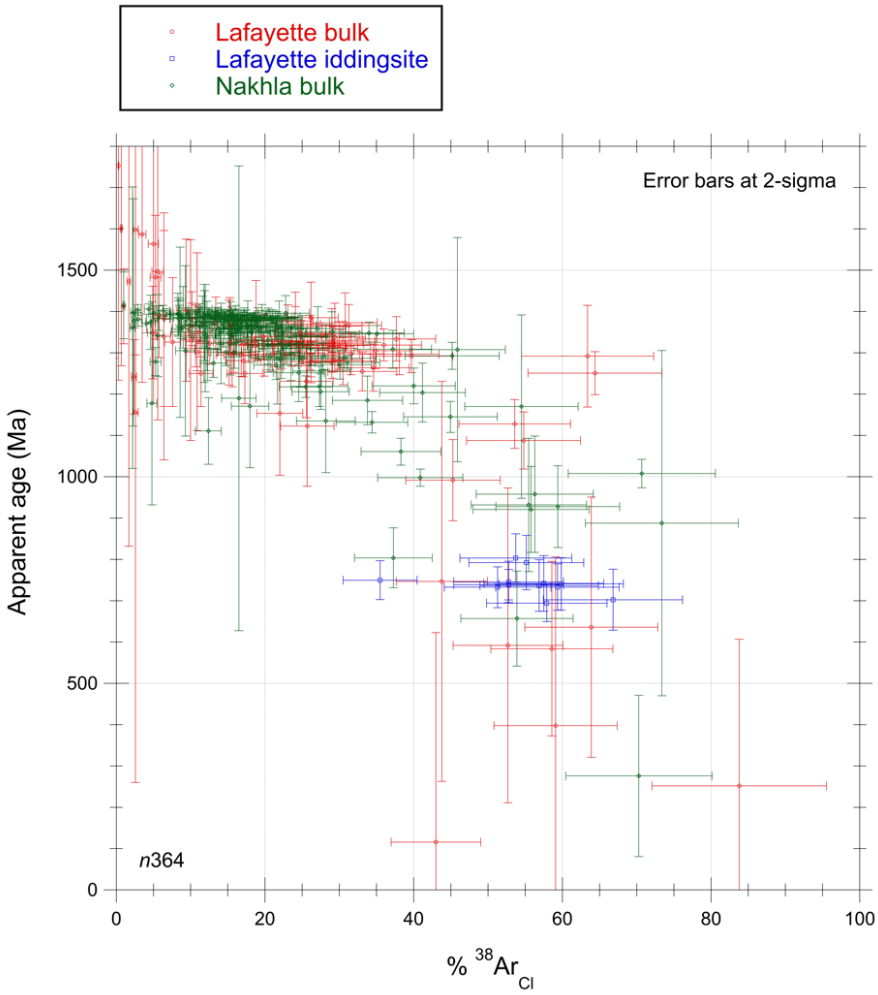

Figure S-3 Apparent $^{40}Ar/^{39}Ar$ age as a function of % $^{38}Ar_{Cl}$ for the Lafayette iddingsite and the bulk-rock step-heating data for Nakhla and Lafayette from Cohen *et al.* (2017). The data show that the low temperature steps from the bulk rock step-heating of Nakhla and Lafayette correlate with the $^{40}Ar/^{39}Ar$ age for the iddingsite as well as the enriched $^{38}Ar_{Cl}$ contents. $^{40}Ar/^{39}Ar$ bulk rock step-heating data yield systematically younger age steps in the first 15 % of ^{39}Ar release and define a mixing relationship between the low-temperature alteration materials and the primary (higher-temperature) igneous component (that defined the age plateaus; Cohen *et al.*, 2017). The youngest ages in the low temperature degassing steps from the bulk measurements are likely an artifact of recoil, as previously suggested (Burgess *et al.*, 2000).

Argon Diffusion Calculations

To evaluate the possibility that different events in the history of Lafayette could have caused partial diffusive loss of radiogenic ^{40}Ar after the iddingsite formed, we performed two different sets of argon diffusion calculations. In the first set of calculations, we model argon diffusive loss for a square pulse heating event, wherein temperature is assumed to instantaneously increase from a temperature below which any diffusion will occur to a constant, higher temperature T (K) for a given duration t (s), and subsequently instantaneously decrease to a temperature below which any diffusion will occur. For this set of calculations, we assume that the duration t of the square pulse heating event is short enough that production of ^{40}Ar by radioactive decay of ^{40}K during the heating event can be ignored. For up to 85 % diffusive loss of argon, the relationship between the fraction of argon lost during such a square pulse heating event and temperature can be expressed as:

$$f \approx \left(\frac{6}{\pi^{\frac{3}{2}}}\right)(\pi^2 F_O)^{\frac{1}{2}} - \left(\frac{3}{\pi^2}\right)(\pi^2 F_O) \quad \text{(S-1)}$$

where F_O, the Fourier number, is equal to:

$$F_O = \frac{D_0 t}{r^2} e^{-E_a/(RT)} \quad \text{(S-2)}$$

and where D_0 is a pre-exponential factor ($cm^2 \cdot s^{-1}$), r is the diffusion length scale (cm) which we assume to be equal to the grain size, E_a is activation energy ($kJ \cdot mol^{-1}$), and R is the gas constant (0.0083145 $kJ \cdot K^{-1} \cdot mol^{-1}$) (McDougall and Harrison, 1999). Equation S-1 can be solved iteratively to determine what temperature, given a specified duration, will produce a given amount of diffusive argon loss. We use these iterative solutions to constrain the duration and temperature combinations that could have caused substantial heating loss from the iddingsite in Lafayette during either its impact ejection event or its atmospheric entry upon falling to Earth, using the diffusion kinetics of muscovite determined experimentally by Harrison *et al.* (2009). We carried out these calculations for two endmember grain sizes (0.01 μm and 10 μm).

In the second set of calculations, we consider a longer-duration event–the 10.7 Myr transit time of Lafayette from its impact ejection from Mars until its atmospheric entry–and therefore do not ignore production of ^{40}Ar by radioactive decay of ^{40}K. Instead, we model the simultaneous production and diffusion of ^{40}Ar under isothermal conditions. These isothermal models represent a reasonable upper bound for the temperatures required to induce partial diffusive loss of the radiogenic argon. This is because for true time-temperature histories along potential orbital trajectories, higher temperatures would be permitted over shorter durations of time. For this set of calculations, we must solve an analytical solution for simultaneous production and diffusion after Wolf *et al.* (1998) that involves two infinite series, which typically converge within 20 partial sums or fewer:

$$t_{app} = \frac{r^2}{D}\left[\frac{1}{15} - \sum_{n=1}^{\infty} \frac{6}{\pi^4 n^4} exp(-n^2\pi^2 F_O)\right] + t_{init} \sum_{n=1}^{\infty} \frac{6}{\pi^2 n^2} exp(-n^2\pi^2 F_O) \quad \text{(S-3)}$$

where t_{app} is the apparent age of the iddingsite (in this case, 742 Ma), and t_{init} is the initial age prior to the onset of isothermal heating (*i.e.* prior to Lafayette's space transit). Like Equation S-1, we can solve Equation S-3 iteratively to map out the grain size and temperature combinations, given an isothermal heating event lasting 10.7 Myr, that would yield a particular fractional argon loss (*i.e.* $1 - t_{app}/t_{init}$). As in the first set of calculations, we used the diffusion kinetics of muscovite determined experimentally by Harrison *et al.* (2009).

Supplementary Tables

Table S-1 Digitized Rb-Sr data from Lafayette (Shih *et al.*, 1998).

Table S-2 Parameter values used in the reduction of $^{40}Ar/^{39}Ar$ data.

Parameter	Value
Isotopic abundances and decay constants (Lee et al., 2006; Renne et al., 2010, 2011)	
$^{40}Ar/^{36}Ar$, Earth's atmosphere	298.56 ± 0.31
$^{40}K/K$	1.167×10^{-4}
$^{40}K\ \lambda_{\varepsilon}$	$(5.757 \pm 0.016) \times 10^{-11}$ a^{-1}
$^{40}K\ \lambda_{\beta}$	$(4.9548 \pm 0.0134) \times 10^{-10}$ a^{-1}
$^{40}K\ \lambda$ total	$(5.5305 \pm 0.0135) \times 10^{-10}$ a^{-1}
$^{37}Ar\ \lambda$	0.01983 ± .0000226 days^{-1}
$^{39}Ar\ \lambda$	$(7.055 \pm 0.039) \times 10^{-6}$ days^{-1}
$^{36}Cl\ \lambda_{\beta}$	$(6.1817 \pm 0.040) \times 10^{-9}$ days^{-1}
Reactor production ratios and interfering isotope production ratios (Renne et al., 2005)	
$(^{36}Cl/^{38}Cl)_{Cl}$	263 ± 2
$(^{38}Ar/^{37}Ar)_{Ca}$	$(1.96 \pm 0.08) \times 10^{-5}$
$(^{38}Ar/^{39}Ar)_{K}$	$(1.22 \pm 0.01) \times 10^{-2}$
$(^{40}Ar/^{39}Ar)_{K}$	$(7.30 \pm 0.92) \times 10^{-4}$
$(^{37}Ar/^{39}Ar)_{K}$	$(2.24 \pm 0.16) \times 10^{-4}$
$(^{39}Ar/^{37}Ar)_{Ca}$	$(6.95 \pm 0.09) \times 10^{-4}$
$(^{36}Ar/^{37}Ar)_{Ca}$	$(2.65 \pm 0.02) \times 10^{-4}$

Table S-3 Argon isotope data from 12 iddingsite aliquots of Lafayette.

Tables S-1 and S-3 are available for download (.xlsx) from the online version of this article at http://doi.org/10.7185/geochemlet.2443.

Supplementary Information References

Bridges, J.C., Grady, M.M. (2000) Evaporite mineral assemblages in the nakhlite (martian) meteorites. *Earth and Planetary Science Letters* 176, 267–279. https://doi.org/10.1016/S0012-821X(00)00019-4

Bridges, J.C., Hicks, L.J., Treiman, A.H. (2019) Carbonates on Mars. In: Filiberto, J., Schwenzer, S.P. (Eds.) *Volatiles in the Martian Crust*. Elsevier, Amsterdam, 89–118. https://doi.org/10.1016/B978-0-12-804191-8.00005-2

Borg, L., Drake, M.J. (2005) A review of meteorite evidence for the timing of magmatism and of surface or near-surface liquid water on Mars. *Journal of Geophysical Research: Planets* 110, E12S03. https://doi.org/10.1029/2005JE002402

Burgess, R., Holland, G., Fernandes, V., Turner, G. (2000) New Ar-Ar Data on Nakhla Minerals. Goldschmidt Conference, 3–8 September 2000, Oxford, UK. *Journal of Conference Abstracts* 5, 266. https://goldschmidtabstracts.info/abstracts/abstractView?id=2000000266

Cassata, W.S., Borg, L.E. (2016) A new approach to cosmogenic corrections in $^{40}Ar/^{39}Ar$ chronometry: Implications for the ages of Martian meteorites. *Geochimica et Cosmochimica Acta* 187, 279–293. https://doi.org/10.1016/j.gca.2016.04.045

Cassata, W.S., Shuster, D.L., Renne, P.R., Weiss, B.P. (2010) Evidence for shock heating and constraints on Martian surface temperatures revealed by $^{40}Ar/^{39}Ar$ thermochronometry of Martian meteorites. *Geochimica et Cosmochimica Acta* 74, 6900–6920. https://doi.org/10.1016/j.gca.2010.08.027

Changela, H.G., Bridges, J.C. (2010) Alteration assemblages in the nakhlites: Variation with depth on Mars. *Meteoritics & Planetary Science* 45, 1847–1867. https://doi.org/10.1111/j.1945-5100.2010.01123.x

Clauer, N., Chaudhuri, S., Kralik, M., Bonnot-Courtois, C. (1993) Effects of experimental leaching on Rb-Sr and K-Ar isotopic systems and REE contents of diagenetic illite. *Chemical Geology* 103, 1–16. https://doi.org/10.1016/0009-2541(93)90287-S

Cohen, B.E., Mark, D.F., Cassata, W.S., Lee, M.R., Tomkinson, T., Smith, C.L. (2017) Taking the pulse of Mars via dating of a plume-fed volcano. *Nature Communications* 8, 640. https://doi.org/10.1038/s41467-017-00513-8

Gyollai, I., Chatzitheodoridis, E., Kereszturi, Á., Szabó, M. (2023) Multiple generation magmatic and hydrothermal processes in a Martian subvolcanic environment based on the analysis of Yamato-000593 nakhlite meteorite. *Meteoritics & Planetary Science* 58, 218–240. https://doi.org/10.1111/maps.13950

Harrison, T.M., Heizler, M.T., Lovera, O.M., Wenji, C., Grove, M. (1994) A chlorine disinfectant for excess argon released from K-feldspar during step heating. *Earth and Planetary Science Letters* 123, 95–104. https://doi.org/10.1016/0012-821X(94)90260-7

Harrison, T.M., Célérier, J., Aikman, A.B., Hermann, J., Heizler, M.T. (2009) Diffusion of ^{40}Ar in muscovite. *Geochimica et Cosmochimica Acta* 73, 1039–1051. https://doi.org/10.1016/j.gca.2008.09.038

Hicks, L.J., Bridges, J.C., Gurman, S.J. (2014) Ferric saponite and serpentine in the nakhlite martian meteorites. *Geochimica et Cosmochimica Acta* 136, 194–210. https://doi.org/10.1016/j.gca.2014.04.010

Kelley, S. (2002) Excess argon in K–Ar and Ar–Ar geochronology. *Chemical Geology* 188, 1–22. https://doi.org/10.1016/S0009-2541(02)00064-5

Krämer Ruggiu, L., Gattacceca, J., Devouard, B., Udry, A., Debaille, V., Rochette, P., Lorand, J.-.-P., Bonal, L., Beck, P., Sautter, V., Busemann, H., Meier, M.M.M., Maden, C., Hublet, G. Martinez, R. (2020) Caleta el Cobre 022 Martian meteorite: Increasing nakhlite diversity. *Meteoritics & Planetary Science* 55, 1539–1563. https://doi.org/10.1111/maps.13534

Lee, J.-Y., Marti, K., Severinghaus, J.P., Kawamura, K., Yoo, H.-S., Lee, J.B., Kim, J.S. (2006) A redetermination of the isotopic abundances of atmospheric Ar. *Geochimica et Cosmochimica Acta* 70, 4507–4512. https://doi.org/10.1016/j.gca.2006.06.1563

Lee, M.R., Tomkinson, T., Mark, D.F., Stuart, F.M., Smith, C.L. (2013) Evidence for silicate dissolution on Mars from the Nakhla meteorite. *Meteoritics & Planetary Science* 48, 224–240. https://doi.org/10.1111/maps.12053

Lee, M.R., Tomkinson, T., Hallis, L.J., Mark, D.F. (2015) Formation of iddingsite veins in the martian crust by centripetal replacement of olivine: Evidence from the nakhlite meteorite Lafayette. *Geochimica et Cosmochimica Acta* 154, 49–65. https://doi.org/10.1016/j.gca.2015.01.022

Lee, M.R., Daly, L., Cohen, B.E., Hallis, L.J., Griffin, S., Trimby, P., Boyce, A., Mark, D.F. (2018) Aqueous alteration of the Martian meteorite Northwest Africa 817: Probing fluid–rock interaction at the nakhlite launch site. *Meteoritics & Planetary Science* 53, 2395–2412. https://doi.org/10.1111/maps.13136

Ludwig, K.R. (2008) Isoplot 3.66: A Geochronological toolkit for Microsoft Excel. *Berkeley Geochronology Center Special Publication* 4, Berkeley.

Mark, D.F., Rice, C.M., Fallick, A.E., Trewin, N.H., Lee, M.R., Boyce, A., Lee, J.K.W. (2011) $^{40}Ar/^{39}Ar$ dating of hydrothermal activity, biota and gold mineralization in the Rhynie hot-spring system, Aberdeenshire, Scotland. *Geochimica et Cosmochimica Acta* 75, 555–569. https://doi.org/10.1016/j.gca.2010.10.014

Martínez, M., Shearer, C.K., Brearley, A.J. (2023) Epitaxial fluorapatite vein in Northwest Africa 998 host apatite: Clues on the geochemistry of late hydrothermal fluids on Mars. *Meteoritics & Planetary Science* 58, 1229–1245. https://doi.org/10.1111/maps.14042

Mattinson, J.M. (1994) A study of complex discordance in zircons using step-wise dissolution techniques. *Contributions to Mineralogy and Petrology* 116, 117–129. https://doi.org/10.1007/BF00310694

McCubbin, F.M., Tosca, N.J., Smirnov, A., Nekvasil, H., Steele, A., Fries, M., Lindsley, D.H. (2009) Hydrothermal jarosite and hematite in a pyroxene-hosted melt inclusion in martian meteorite Miller Range (MIL) 03346: Implications for magmatic-hydrothermal fluids on Mars. *Geochimica et Cosmochimica Acta* 73, 4907–4917. https://doi.org/10.1016/j.gca.2009.05.031

McDougall, I., Harrison, T.M. (1999) *Geochronology and Thermochronology by the $^{40}Ar/^{39}Ar$ Method*. Second Edition, Oxford University Press, New York.

Misawa, K., Shih, C.-Y., Wiesmann, H., Garrison, D.H., Nyquist, L.E., Bogard, D.D. (2005) Rb-Sr, Sm-Nd and Ar-Ar isotopic systematics of Antarctic nakhlite Yamato 000593. *Antarctic Meteorite Research* 18, 133–151.

Nyquist, L.E., Takeda, H., Bansal, B.M., Shih, C.-Y., Wiesmann, H., Wooden, J.L. (1986) Rb-Sr and Sm-Nd internal isochron ages of a subophitic basalt clast and a matrix sample from the Y75011 eucrite. *Journal of Geophysical Research: Solid Earth* 91, 8137–8150. https://doi.org/10.1029/JB091iB08p08137

Piercy, J.D., Bridges, J.C., Hicks, L.J. (2022) Carbonate dissolution and replacement by odinite and saponite in the Lafayette nakhlite: Part of the CO_2-CH_4 cycle on Mars? *Geochimica et Cosmochimica Acta* 326, 97–118. https://doi.org/10.1016/j.gca.2022.02.003

Renne, P.R., Knight, K.B., Nomade, S., Leung, K.-N. Lou, T.-P. (2005) Application of deuteron-deuteron (D-D) fusion neutrons to $^{40}Ar/^{39}Ar$ geochronology. *Applied Radiation and Isotopes* 62, 25–32. https://doi.org/10.1016/j.apradiso.2004.06.004

Renne, P.R., Mundil, R., Balco, G., Min, K., Ludwig, K.R. (2010) Joint determination of ^{40}K decay constants and $^{40}Ar^*/^{40}K$ for the Fish Canyon sanidine standard, and improved accuracy for $^{40}Ar/^{39}Ar$ geochronology. *Geochimica et Cosmochimica Acta* 74, 5349–5367. https://doi.org/10.1016/j.gca.2010.06.017

Renne, P.R., Balco, G., Ludwig, K.R., Mundil, R., Min, K. (2011) Response to the comment by W.H. Schwarz et al. on "Joint determination of ^{40}K decay constants and $^{40}Ar^*/^{40}K$ for the Fish Canyon sanidine standard, and improved accuracy for $^{40}Ar/^{39}Ar$ geochronology" by P.R. Renne et al. (2010). *Geochimica et Cosmochimica Acta* 75, 5097–5100. https://doi.org/10.1016/j.gca.2011.06.021

Rotenberg, E., Davis, D.W., Amelin, Y., Ghosh, S., Bergquist, B.A. (2012) Determination of the decay-constant of ^{87}Rb by laboratory accumulation of ^{87}Sr. *Geochimica et Cosmochimica Acta* 85, 41–57. https://doi.org/10.1016/j.gca.2012.01.016

Shih, C.-Y., Nyquist, L.E., Reese, Y., Wiesmann, H. (1998) The Chronology of the Nakhlite, Lafayette: Rb-Sr and Sm-Nd Isotopic Ages. *Lunar and Planetary Science Conference XXIX*, abstract 1145.

Shih, C.-Y., Nyquist, L.E., Wiesmann, H. (1999) Samarium-neodymium and rubidium-strontium systematics of nakhlite Governador Valadares. *Meteoritics & Planetary Science* 34, 647–655. https://doi.org/10.1111/j.1945-5100.1999.tb01370.x

Shih, C.Y., Wiesmann, H., Nyquist, E.L. Misawa, K. (2002) Crystallization age of Antarctic nakhlite Y000593: Further evidence of nakhlite launch pairing. *Antarctic Meteorites XXVII*, 151–153.

Steiger, R.H., Jäger, E. (1977) Subcommission on geochronology: Convention on the use of decay constants in geo- and cosmochemistry. *Earth and Planetary Science Letters* 36, 359–362. https://doi.org/10.1016/0012-821X(77)90060-7

Tomkinson, T., Lee, M.R., Mark, D.F., Smith, C.L. (2013) Sequestration of Martian CO_2 by mineral carbonation. *Nature Communications* 4, 2662. https://doi.org/10.1038/ncomms3662

Treiman, A.H. (2005) The nakhlite meteorites: Augite-rich igneous rocks from Mars. *Geochemistry* 65, 203–270. https://doi.org/10.1016/j.chemer.2005.01.004

Treiman, A.H., Barrett, R.A., Gooding, J.L. (1993) Preterrestrial aqueous alteration of the Lafayette (SNC) meteorite. *Meteoritics* 28, 86–97. https://doi.org/10.1111/j.1945-5100.1993.tb00251.x

Vermeesch, P. (2018) IsoplotR: A free and open toolbox for geochronology. *Geoscience Frontiers* 9, 1479–1493. https://doi.org/10.1016/j.gsf.2018.04.001

Wolf, R.A., Farley, K.A., Kass, D.M. (1998) Modeling of the temperature sensitivity of the apatite (U–Th)/He thermochronometer. *Chemical Geology* 148, 105–114. https://doi.org/10.1016/S0009-2541(98)00024-2

York, D., Evensen, N.M., Martínez, M.L., De Basabe Delgado, J. (2004) Unified equations for the slope, intercept, and standard errors of the best straight line. *American Journal of Physics* 72, 367–375. https://doi.org/10.1119/1.1632486